arXiv:cond-mat/0305248v2 [cond-mat.stat-mech] 28 Aug 2003

A column of grains in the jamming limit: glassy dynamics in the compaction process

J.M. Luck[a,1] and Anita Mehta[b,2]

[a]Service de Physique Théorique[3], CEA Saclay, 91191 Gif-sur-Yvette cedex, France
[b]S.N. Bose National Centre for Basic Sciences, Block JD, Sector 3, Salt Lake, Calcutta 700098, India

Abstract

We investigate a stochastic model describing a column of grains in the jamming limit, in the presence of a low vibrational intensity. The key control parameter of the model, ε, is a representation of granular shape, related to the reduced void space. Regularity and irregularity in grain shapes, respectively corresponding to rational and irrational values of ε, are shown to be centrally important in determining the statics and dynamics of the compaction process.

P.A.C.S.: 45.70.–n, 45.70.Cc, 45.70.Mg

[1]luck@spht.saclay.cea.fr
[2]anita@boson.bose.res.in
[3]URA 2306 of CNRS

1 Introduction

The study of slow dynamics in the jamming limit unifies the fields of granular compaction [1, 2] and glasses [3]. Key features of this involve frustration and hysteresis, among other complex phenomena [4], with the concomitant difficulty of modelling them in simple and physical ways. We present in the following a model of remarkable simplicity, which is nevertheless able to capture to a large extent the complex consequences of non-trivial interactions, *even in one dimension*. Issues that are probed include the effects of orientation, and thus shape, on packing in the jamming limit. 'Irregular' and 'regular' shapes of units (for example, grains) will be seen to have rather different consequences for compaction behaviour, when they are subjected to zero- and low-temperature dynamics.

The present model is an extension, with interactions, of an earlier model of noninteracting grains, presented in [5]. For clarity, we summarise in what follows the commonality and differences between the two. The previous model was two-dimensional. Each lattice site was occupied by an ordered grain (+), a disordered grain (−), or a hole (0). It interpolated between a fluidised regime, where there were many holes on the lattice, and a jammed regime, where there were no holes anywhere on the lattice. The restricted dynamics in the jammed regime forbade migration of grains anywhere on the two-dimensional lattice, and in particular between columns. The result was expressible in terms of a column model of noninteracting grains, with a (trivial) ground state of completely ordered (+) grains. This, surprisingly, nevertheless exhibited some features usually associated with glassiness, such as slow dynamics and aging [5].

Clearly, disordered systems such as glasses or jammed granular media do not have ground states that are crystalline; equally, their attempts to reach their ground states are mediated by complex long-range interactions. The present model, already introduced in [6] and investigated to some extent in [7], represents an effort to make the jammed limit of the earlier model more realistic, by the inclusion of interactions. The column contains no holes. Each grain is either ordered (represented by a (+) Ising spin) or disordered (represented by a (−) spin). However, and differently from the previous model, we take into account the effect of voids (holes that *partially* occupy a lattice site) which are associated with each disordered orientation of a grain. Thus, while each ordered grain fully occupies one unit of space, each disordered grain occupies ε units of space, so that $(1-\varepsilon)$ is a measure of the trapped void space. The net volume occupied by a disordered grain, or the corresponding void space, will depend on its shape; we see that ε *is thus a simple representation of granular shape*. Also, and differently from the earlier model, the process of compaction is now no longer a simple relaxation into a completely ordered state: a given distribution of (+) and (−) grains, as in nature, responds to externally imposed dynamics, by minimising void space *locally*, in the presence of disorder. The ground states so obtained resemble much more the random close-packed state found in granular systems [8] than the rather unrealistic crystalline state (all grains ordered) obtained before.

2 The model

Our model is a fully directed model of interacting grains, where causality induces a directionality both in time and in space, as the orientation of a given grain only influences the grains *below* it, and at *later* times. Grains occupy all N sites of a column. As said above, we assume that they only assume two orientational states. We set $\sigma_n = +1$ (resp. $\sigma_n = -1$) if grain n is ordered (resp. disordered). A configuration of the system is uniquely defined by the orientation variables $\{\sigma_n\}$.

It is known [9, 10] that the response of jammed granular media to low-amplitude vibration is compacting; that is, grains rearrange themselves to locally maximise their packing fraction or, equivalently, minimise their void space. We model this by a local stepwise compacting dynamics: that is, a given grain orients itself to minimise void space *locally*, given the orientations of grains above itself.

To be more specific, in the presence of a dimensionless vibration intensity Γ, we consider a stochastic dynamics, defined by the orientation-flipping rates

$$\begin{cases} w_n(+ \to -) = \exp(-(\lambda_n + h_n)/\Gamma), \\ w_n(- \to +) = \exp(-(\lambda_n - h_n)/\Gamma). \end{cases} \tag{2.1}$$

In these expressions, h_n and λ_n are, respectively, the local ordering field and the activation energy felt by grain n. These quantities are assumed to only depend on the orientations of grains *above* grain n.

We make the further simplifying assumption that the activation energy λ_n does not depend on grain orientations at all. We write

$$\lambda_n = n\Gamma/\xi_{\rm dyn}, \tag{2.2}$$

where $\xi_{\rm dyn}$ is defined to be the *dynamical length* [see (2.6)]. Roughly speaking, $\xi_{\rm dyn}$ is the depth of the nonequilibrium boundary layer: grains which are well within this length can order relatively freely in response to surface events, while grains much deeper relax only logarithmically in time [5].

The only dependence of the dynamics on orientations is via the ordering field h_n, which determines the orientational response of grain n to orientations of grains above it. We choose to write the simple, linear formula

$$h_n = \varepsilon m_n^- - m_n^+, \tag{2.3}$$

where m_n^+ and m_n^- are the numbers of ordered and disordered grains above grain n:

$$m_n^+ = \frac{1}{2}\sum_{k=1}^{n-1}(1+\sigma_k), \qquad m_n^- = \frac{1}{2}\sum_{k=1}^{n-1}(1-\sigma_k). \tag{2.4}$$

In spite of its simplicity, the dynamics defined by (2.1)–(2.3) can be shown to capture the compaction mechanism sketched in the Introduction, namely a local minimisation of the *excess void space* [11]. In particular, a transition from the ordered to the disordered

state for grain n is *hindered* by the number of voids that are already above it. The whole picture will become clearer with the example of $\varepsilon = 1/2$, discussed in section 3.2.

In order to perform numerical Monte-Carlo simulations we will need a discrete-time formulation of the above rules. The flipping rates w_n become flipping probabilities

$$\begin{cases} p_n(+ \to -) = \dfrac{P_n}{1 + \exp(2h_n/\Gamma)}, \\ p_n(- \to +) = \dfrac{P_n}{1 + \exp(-2h_n/\Gamma)}, \end{cases} \tag{2.5}$$

where the factor

$$P_n = \exp(-\lambda_n/\Gamma) = \exp(-n/\xi_{\rm dyn}) \tag{2.6}$$

describes the *a priori* exponential slowing down of the dynamics with depth n.

Throughout the following, ε, $\xi_{\rm dyn}$, and Γ (the latter being referred to as 'temperature') will be considered as three independent parameters of the model. In particular, ε will not necessarily be restricted to the range $0 < \varepsilon < 1$, suggested by the interpretation of $(1 - \varepsilon)$ as the trapped void space.

The zero-temperature statics and dynamics will crucially depend on whether ε is rational or irrational. Arguing that rational and irrational ε corresponds to smooth/regular and rough/irregular shapes, respectively, this difference is to be expected, and will be discussed further.

3 Zero-temperature statics

As the dynamical rules (2.1) are fully directional, they clearly cannot obey detailed balance. The dynamics simplifies, however, in the $\Gamma \to 0$ limit [6], where (2.1) yields

$$\frac{w_n(- \to +)}{w_n(+ \to -)} = \exp(2h_n/\Gamma) \to \begin{cases} \infty & \text{if} \quad h_n > 0, \\ 0 & \text{if} \quad h_n < 0. \end{cases} \tag{3.1}$$

From a purely *static* viewpoint, *ground states* of the system can therefore be defined by the condition that the orientation of every grain is aligned along its local field, according to the deterministic equation:

$$\sigma_n = \operatorname{sign} h_n = \begin{cases} + & \text{if} \quad h_n > 0, \\ - & \text{if} \quad h_n < 0, \end{cases} \tag{3.2}$$

provided $h_n \neq 0$ (see below). The condition (3.2) only involves the parameter ε [see (2.3)]. It is recursive, because of directionality, in that the right-hand side at depth n only involves the upper grains $k = 1, \ldots, n-1$. The uppermost orientation σ_1 is left unspecified, as the corresponding local field vanishes identically. In the following, we assume for definiteness that the uppermost grain is ordered:

$$\sigma_1 = +. \tag{3.3}$$

It turns out that the zero-temperature rule (3.2) yields a rich ground-state structure, because of subtle commensurability and frustration effects. Our starting point is to observe that (3.2) implies

$$\begin{cases} h_n > 0 \Longrightarrow \sigma_n = +, & m_{n+1}^+ = m_n^+ + 1, & m_{n+1}^- = m_n^-, & h_{n+1} = h_n - 1, \\ h_n < 0 \Longrightarrow \sigma_n = -, & m_{n+1}^+ = m_n^+, & m_{n+1}^- = m_n^- + 1, & h_{n+1} = h_n + \varepsilon. \end{cases} \tag{3.4}$$

The number and the nature of ground states depend on whether ε is rational or irrational, which we consider separately below.

3.1 Irrational ε: unique quasiperiodic ground state

Irrational values of ε imply, in qualitative terms, a strong irregularity of grain shape. We refer to this as 'roughness'. Below, we demonstrate that the ground state of a packing of rough grains is unique, and optimally, but not maximally packed. We can visualise this as the interlocking of jutting edges to minimise, but not eliminate, voids.

For irrational ε, (3.4) implies recursively that all the local fields h_n are non-zero, and that they lie in the bounded interval

$$-1 \leq h_n \leq \varepsilon. \tag{3.5}$$

Let us introduce the following *superspace formalism*. Consider the integers (m_n^-, m_n^+) as the co-ordinates of points on a square lattice. We thus obtain a broken, staircase-shaped line, starting as $(m_1^-, m_1^+) = (0, 0)$, $(m_2^-, m_2^+) = (0, 1)$ [see (3.3)], etc. Vertical steps correspond to ordered $(+)$ grains, whereas horizontal steps correspond to disordered $(-)$ grains. Equation (3.5) defines an oblique strip with *slope* ε in the (m^-, m^+) plane, which contains the entire broken line thus constructed (see Figure 1).

A unique infinite configuration of grain orientations (i.e., a unique broken line) is thus generated. This configuration is *quasiperiodic*. Indeed the above construction is equivalent to the cut-and-project method of generating quasiperiodic tilings of the line, which has been extensively studied [12] in the framework of quasicrystals. (Had we made the initial choice $\sigma_1 = -$ instead of (3.3), we would have obtained the same quasiperiodic configuration, up to a permutation of the two uppermost grains.) We mention for further reference the following explicit expressions[1] for $m_n^\pm$ and h_n:

$$m_n^+ = n - m_n^- = 1 + \mathrm{Int}((n-1)\Omega), \qquad h_n = -1 + \frac{\mathrm{Frac}((n-1)\Omega)}{1-\Omega}, \tag{3.6}$$

where the rotation number Ω reads

$$\Omega = \varepsilon/(1+\varepsilon). \tag{3.7}$$

[1] $\mathrm{Int}(x)$, the integer part of a real number x, is the largest integer less than or equal to x, and $\mathrm{Frac}(x) = x - \mathrm{Int}(x)$ is the fractional part of x $(0 \leq \mathrm{Frac}(x) < 1)$.

An immediate consequence of (3.6) is that there are well-defined proportions of ordered and disordered grains in the ground state:

$$f_+ = \Omega = \varepsilon/(1+\varepsilon), \qquad f_- = 1 - \Omega = 1/(1+\varepsilon). \tag{3.8}$$

This geometrical construction is illustrated in Figure 1 for the most familiar irrational number, the inverse golden mean [13]:

$$\varepsilon = \Phi - 1 = 1/\Phi, \qquad \Omega = 2 - \Phi = 1/\Phi^2, \qquad \Phi = (\sqrt{5}+1)/2 \approx 1.618033. \tag{3.9}$$

The corresponding grain configuration is given by a Fibonacci sequence [12, 13]:

$$\{\sigma_n\} = + - - + - - + - + - - + - - + - + - - + - + - - \cdots$$

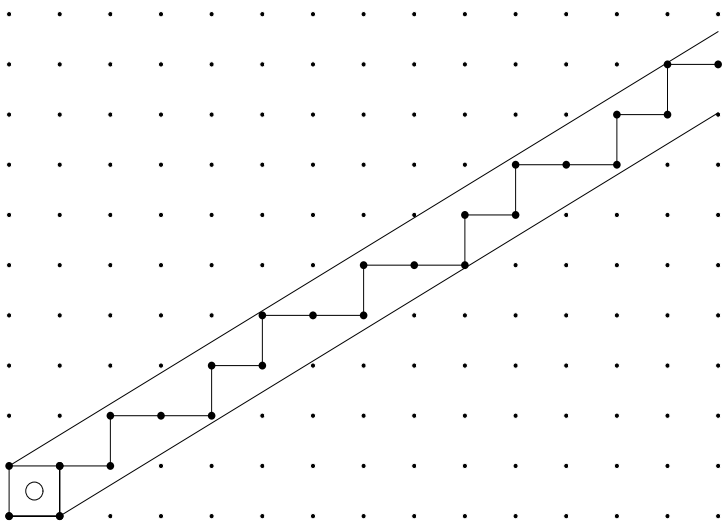


Figure 1: Geometrical construction of the quasiperiodic ground state of the model for the golden-mean slope (3.9). The two ways of going around the first cell, marked with a circle, correspond to the two possible choices for the orientation of the uppermost grain.

To recapitulate, at any point in the ground state, the ordering field h_n will assume a finite, non-zero value, implying in its turn a given orientation of the grain that follows. The process is therefore fully deterministic, and the state obtained, unique. We will see that things will be rather different for rational values of ε.

3.2 Rational ε: degenerate ground states

Rational values of ε imply, in qualitative terms, a regularity of grain shape or of void space, which we term 'smoothness'. We might here expect that regularly shaped grains could align themselves to fit into accumulated void space, in a given ground state configuration; this in fact happens, leading to states of perfect packing at various points of

the column. This in turn gives rise to the observed degeneracy of ground states to be discussed further below.

For a rational ε:

$$\varepsilon = p/q, \qquad \Omega = p/(p+q), \tag{3.10}$$

in irreducible form (p and q are mutual primes), some of the local fields h_n generated by the recursion equations (3.4) vanish. The corresponding grain orientations σ_n remain unspecified. This means that grain n has a perfectly packed column above it, so that it is free to choose its orientation. For $\varepsilon = 1/2$, for example, one can visualise that each disordered grain 'carries' a void half its size, so that units of perfect packing must be permutations of the triad $+--$, where the two 'half' voids from each of the $(-)$ grains are filled by the $(+)$ grain. (Evidently this is a one-dimensional interpretation of packing, so that the serial existence of two half voids and a grain should be interpreted as the insertion of a grain into a full void in higher dimensions.) The dynamics, which is *stepwise compacting*, selects only two of these patterns, $+--$ and $-+-$ (see the second line of Table 1).

This feature of rational slopes is clearly visible on the geometrical construction. Figure 2, corresponding to $\varepsilon = 2/3$, shows that some of the lattice cells, marked with circles, are entirely contained in the closed strip (3.5). Consider one such cell. The broken line enters the cell at its lower left corner and exits the cell at its upper right corner. It can go either counterclockwise, via the lower right corner, giving $\sigma_{n+1} = -$, $\sigma_{n+2} = +$, or clockwise, via the upper left corner, giving $\sigma_{n+1} = +$, $\sigma_{n+2} = -$. Each marked cell thus generates a binary choice in the construction. This orientational indeterminacy occurs at points of perfect packing, such that n is a multiple of the *period* $p+q$, equal to the denominator of the rotation number Ω. The model therefore has a non-zero ground-state entropy, or zero-temperature configurational entropy, $\Sigma = \ln 2/(p+q)$ per grain. Each ground state is a random sequence of two well-defined patterns of length $p+q$, each of them made of p ordered and q disordered ones, so that (3.8) still holds for each of the ground states. The patterns only differ by their first two orientations. The first cases are listed in Table 1. Finally, the period $p+q$ is formally infinite for an irrational slope. Accordingly, there is only one marked cell in Figure 1, for $n = 0$, corresponding to the fact that only the uppermost grain is unspecified.

4 Zero-temperature dynamics

Zero-temperature dynamics is a priori the canonical way of retrieving the ground states of a system. Here, the rule for zero-temperature dynamics is:

$$\sigma_n \to \operatorname{sign} h_n, \tag{4.1}$$

according to (3.1), with the definition (2.3). We will find that irregular grains are able to retrieve their unique ground state, but that the degeneracy of the ground states for regularly shaped grains will make them impossible to retrieve. In the latter case, we find

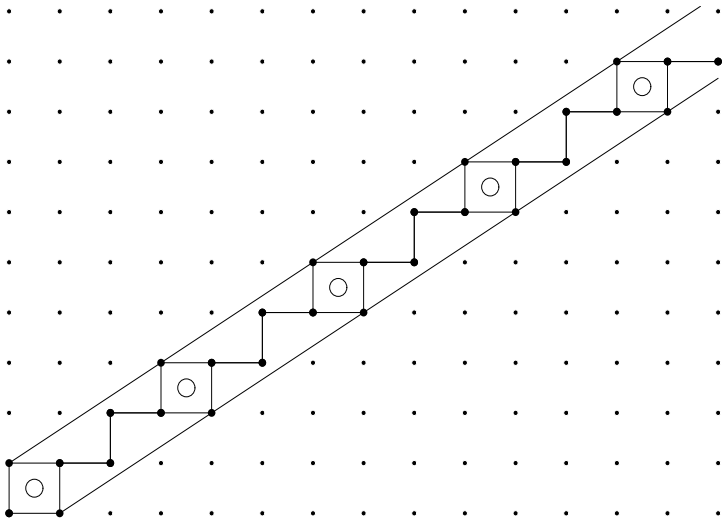


Figure 2: Geometrical construction of the ground states of the model for the rational slope $\varepsilon = 2/3$. The marked cells, entirely contained in the strip, are responsible for the non-zero configurational entropy.

instead a steady state with non-trivial *density fluctuations* above the ground states, which recall the observed density fluctuations above the random close-packed state [9, 10].

4.1 Irrational ε, infinite $\xi_{\rm dyn}$: ballistic coarsening

For irrational ε, the rule (4.1) is always well-defined, as the local fields h_n never vanish. We start with the situation where $\xi_{\rm dyn}$ is infinite. We assume that the system is initially in a disordered state, where each grain is oriented at random: $\sigma_n = \pm$ with equal probabilities, except for the uppermost one, which is fixed according to (3.3).

The zero-temperature dynamics is observed to drive the system to its quasiperiodic ground state. This ordering propagates down the system from its top surface, via *ballistic coarsening*. At time t, the grain orientations have converged to their ground-state values, given by the above geometrical construction, in an upper layer whose depth is observed to grow linearly with time:

$$L(t) \approx Vt, \tag{4.2}$$

whereas the rest of the system is still nearly in its disordered initial state.

This phenomenon is similar to phase ordering, as order propagates over a macroscopic length $L(t)$ which grows forever. It is however different from usual coarsening, as the depth of the ordered region grows ballistically, vith a well-defined ε-dependent ordering velocity V, instead of diffusively, or even more slowly [14]. Figure 3 shows a plot of the inverse of the ordering velocity, measured in a numerical simulation, against ε, for $0 < \varepsilon < 1$. The ordering velocity obeys the symmetry property $V(\varepsilon) = V(1/\varepsilon)$. It is observed to vary smoothly with ε (although it is only defined for irrational ε), and to diverge as $V \sim 1/\varepsilon$ as $\varepsilon \to 0$.

period $p+q$	rot. number Ω	slope ε	p	q	pattern 1	pattern 2
2	1/2	1	1	1	$+-$	$-+$
3	1/3	1/2	1	2	$+--$	$-+-$
3	2/3	2	2	1	$+-+$	$-++$
4	1/4	1/3	1	3	$+---$	$-+--$
4	3/4	3	3	1	$+-++$	$-+++$
5	1/5	1/4	1	4	$+----$	$-+---$
5	2/5	2/3	2	3	$+--+-$	$-+-+-$
5	3/5	3/2	3	2	$+-+-+$	$-++-+$
5	4/5	4	4	1	$+-+++$	$-++++$
6	1/6	1/5	1	5	$+-----$	$-+----$
6	5/6	5	5	1	$+-++++$	$-+++++$

Table 1: Patterns building up the random ground states for the first rational values of ε. The second example with period 5 is illustrated in Figure 2.

4.2 Irrational ε, finite $\xi_{\rm dyn}$: crossover to logarithmic coarsening

For irrational ε, in the situation where $\xi_{\rm dyn}$ is finite, but large at the microscopic scale of a grain, the ballistic coarsening law (4.2) is to be modified as $\mathrm{d}L/\mathrm{d}t \approx V\,\exp(-L/\xi_{\rm dyn})$, taking the slowing down factor (2.6) into account, hence

$$L(t) \approx \xi_{\rm dyn} \ln(1 + Vt/\xi_{\rm dyn}). \tag{4.3}$$

Equation (4.3) exhibits a crossover between the ballistic law (4.2) for $1 \ll Vt \ll \xi_{\rm dyn}$, and the logarithmic coarsening law

$$L(t) \approx \xi_{\rm dyn} \ln t, \tag{4.4}$$

already present in the model of non-interacting grains [5, 6]. The dynamical length $\xi_{\rm dyn}$ thus controls the spatial dependence of dynamical behaviour. In earlier work [5] it was shown to determine the extent to which order propagates down the column, in the glassy regime. This interpretation in terms of an *ordered boundary layer* continues to be valid in the present case: For an initially disordered state, the application of zero-temperature dynamics causes the quasiperiodic ground state to be recovered downwards from the free surface to a depth which grows ballistically with time. When $L(t)$ becomes comparable with $\xi_{\rm dyn}$, the effects of the free surface begin to be damped, and in particular, for $t \gg \xi_{\rm dyn}/V$, one recovers the logarithmic law (4.4), widely associated with the slow dynamical relaxation of vibrated sand [9].

Equation (4.3) has been checked against the results of accurate numerical simulations, for the golden-mean slope. Figure 4 shows a scaling plot of numerical data for $L(t)$ corresponding to $\xi_{\rm dyn} = 50$ and 100, together with the prediction (4.3), with no adjustable parameter. The ordering velocity $V \approx 2.58$ is taken from the data of Figure 3.

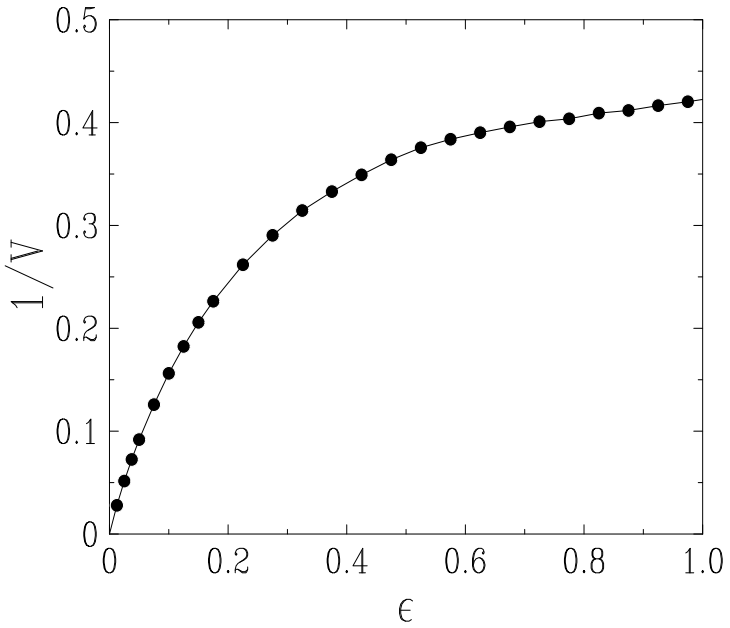


Figure 3: Plot of the inverse ordering velocity $1/V$ of zero-temperature coarsening dynamics at infinite $\xi_{\rm dyn}$, against the irrational slope ε, for $0 < \varepsilon < 1$.

4.3 Rational ε, infinite $\xi_{\rm dyn}$: anomalous roughening

We now turn to zero-temperature dynamics for rational ε. The updating rule (4.1) is not always well-defined as it stands, as the local fields h_n may now vanish. In such a circumstance, it is natural to choose the corresponding orientation at random:

$$\sigma_n \to \begin{cases} + & \text{if} \quad h_n > 0, \\ \pm \text{ with prob. } 1/2 & \text{if} \quad h_n = 0, \\ - & \text{if} \quad h_n < 0. \end{cases} \tag{4.5}$$

The zero-temperature dynamics defined in this way therefore keeps a stochastic component. We focus our attention onto the simplest rational case, i.e., $\varepsilon = 1$. Equation (2.3) for the local fields reads

$$h_n = -\sum_{m=1}^{n-1} \sigma_m. \tag{4.6}$$

We consider first the case where $\xi_{\rm dyn}$ is infinite. We observe that the zero-temperature dynamics (4.5) does not drive the system to any of its degenerate dimerised ground states. The system rather shows a fast relaxation to a unique, non-trivial steady state, independent of the initial state. We now investigate this novel kind of zero-temperature steady state in some detail.

Density fluctuations

First of all, the local field h_n has unbounded fluctuations in the steady state. Figure 5 shows that these fluctuations have a Gaussian distribution of width W_n, at least deep

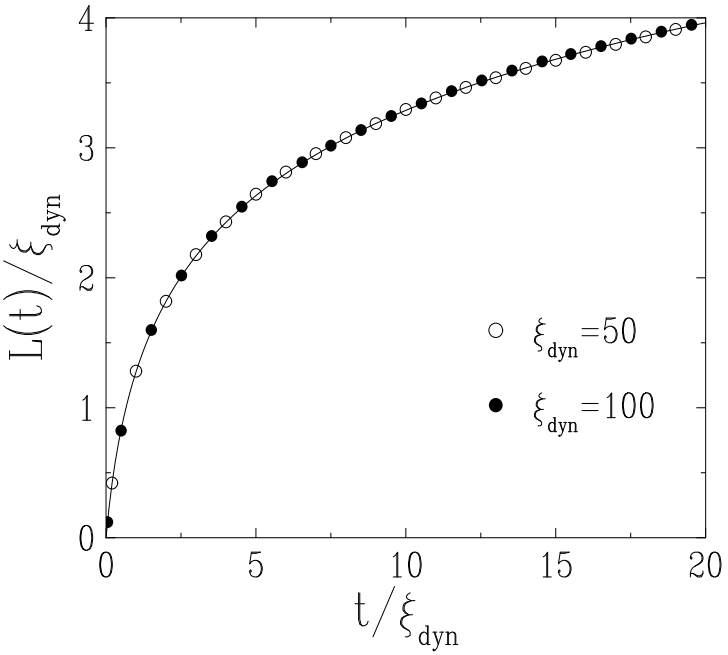


Figure 4: Scaling plot of $L(t)/\xi_{\rm dyn}$ against $t/\xi_{\rm dyn}$ for zero-temperature coarsening dynamics with the golden-mean slope. Symbols: numerical data. Full line: prediction (4.3), with $V = 2.58$.

enough in the system ($n \gg 1$), except for a definite excess of small values of the local field: $|h_n| \sim 1 \ll W_n$. Figure 6 (already shown in [7] and reproduced here for completeness) demonstrates that the local field variance grows as

$$W_n^2 = \langle h_n^2 \rangle \approx A\, n^{2/3}, \tag{4.7}$$

with $A \approx 0.83$.

The exponent 2/3 of the *anomalous roughening* law (4.7) can be explained by means of the following local Markovian approximation. Assume that the local field h_n obeys an effective Langevin equation of the form

$$\mathrm{d}h_n/\mathrm{d}t = -a_n h_n + \eta_n(t), \tag{4.8}$$

where $\eta_n(t)$ is a white noise so that $\langle \eta_n(t)\eta_n(t')\rangle = 2D_n\,\delta(t-t')$. Thus $h_n(t)$ is a Gaussian variable, whose steady-state width W_n is given by the Einstein relation:

$$W_n^2 = \langle h_n^2 \rangle = D_n/a_n. \tag{4.9}$$

The effective parameters a_n and D_n can be estimated as follows. For the deterministic part, (4.5) implies

$$\mathrm{d}\langle h_n\rangle/\mathrm{d}t = \sum_{m=1}^{n-1} \langle \sigma_m - \mathrm{sign}\, h_m \rangle \approx -(1-Q_n)\langle h_n\rangle, \tag{4.10}$$

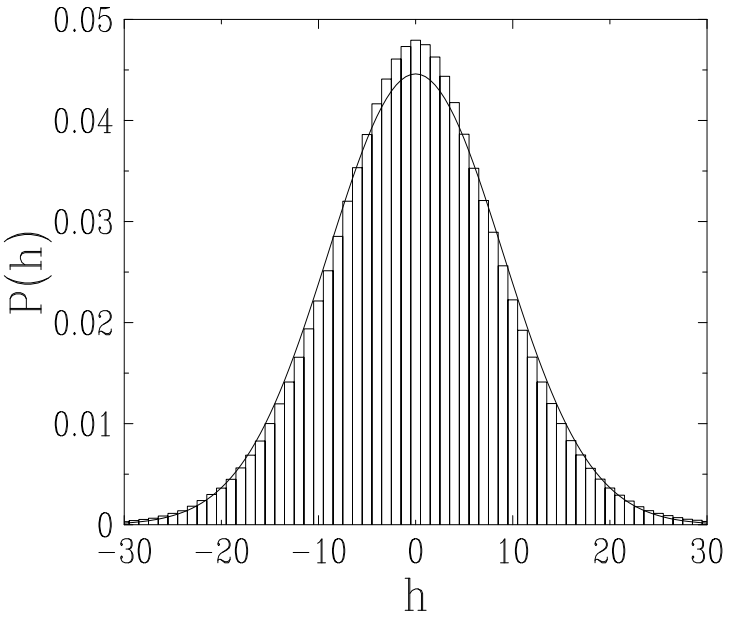


Figure 5: Plot of the distribution of the local field h_n for $n \approx 1000$. Histogram: numerical data (data for $n = 999$ and $n = 1000$ are mixed in order to avoid spurious parity effects). Full curve: Gaussian law with width $W_{1000} = 8.94$.

where the order parameter Q_n is defined as

$$Q_n = \langle \sigma_n \operatorname{sign} h_n \rangle. \tag{4.11}$$

The latter quantity will be shown below to fall off as $n^{-1/3}$ [see (4.22)], implying $a_n \approx 1$. The absence of divergence of the relaxation time $\tau_n = 1/a_n$ with n explains the observed fast relaxation to the steady state. As the fluctuating part is due to the second line of (4.5), the strength of the noise D_n reads, in some units,

$$D_n \approx b \sum_{m=1}^{n-1} \mathrm{Prob}\{h_m = 0\} \approx \frac{b}{\sqrt{2\pi}} \sum_{m=1}^{n-1} \frac{1}{W_m}, \tag{4.12}$$

assuming that the h_n have a Gaussian distribution. Equation (4.9) yields

$$W_n^2 \approx \frac{b}{\sqrt{2\pi}} \sum_{m=1}^{n-1} \frac{1}{W_m}, \tag{4.13}$$

hence the power law (4.7), with $A = (9b^2/(8\pi))^{1/3}$.

The anomalous roughening law (4.7) for the fluctuations of the ordering field h_n is the most central feature of the zero-temperature steady state observed for rational ε. It implies that, unless arranged by hand, the known ground states of a system of regularly shaped objects (i.e., the crystalline ground states) will never be retrieved. On the contrary, the steady state will be one of *density fluctuations* above the ground state (which are related to fluctuations of the excess void space). The present model, to our

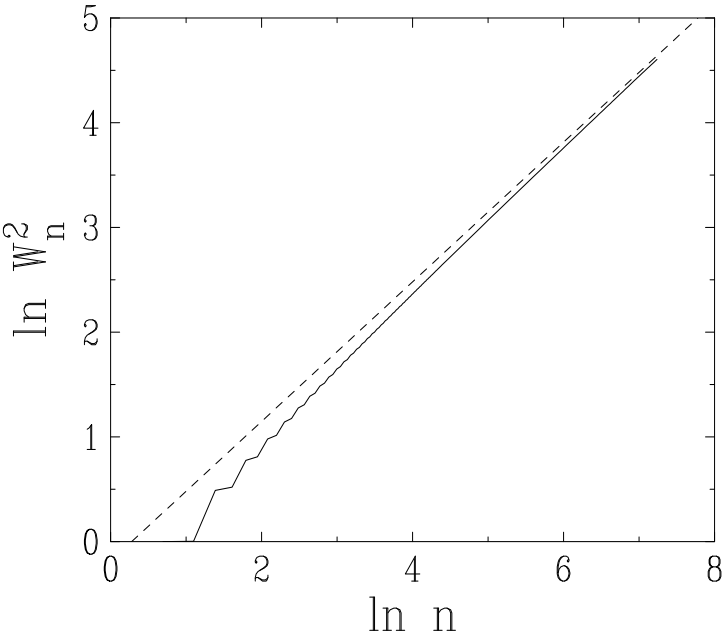


Figure 6: Log-log plot of $W_n^2 = \langle h_n^2 \rangle$ against depth n, for zero-temperature dynamics with $\varepsilon = 1$. Full line: numerical data. Dashed line: fit to asymptotic behaviour, leading to (4.7) (after [7]).

knowledge, thus contains the first derivation of a possible source of density fluctuations in granular media [9, 10], which, here, arise quite naturally from the effect of shape.

These anomalous fluctuations can be put in perspective with two different physical situations. First, as already underlined in [7], the power law (4.7) is reminiscent of the domain-growth mechanism in the low-temperature coarsening regime of the Ising chain with Kawasaki dynamics [15]. Second, using n to represent time in a random walk, the above results could be used to explain the $R_n^2 \approx n^{2/3}$ law recently observed in two-dimensional simulations of the effect of shape in particulate cages [16].

Orientation and local field correlations

If the grain orientations were statistically independent, i.e., uncorrelated, one would have the simple result $\langle h_n^2 \rangle = n\varepsilon$, while (4.7) implies that $\langle h_n^2 \rangle$ grows much more slowly than n. The orientational displacements of each grain are therefore *fully anticorrelated*. The anticorrelated orientational displacements are reminiscent of the *bridge collapse* seen in displacement-displacement correlations of strongly compacting grains [10]; grain orientational displacements in the direction of vibration were there seen to be strongly anticorrelated in jammed regions, as each grain tried to collapse into the void space trapped by its neighbours. Interestingly, correlations *transverse* to the shaking direction were [10] found to be rather small, thus, in self-consistency terms justifying the choice of a column model in the present case. Once again, if we adopt a kinetic viewpoint and treat n as time in a random walk, these anticorrelations recall the temporal anticorrela-

tions observed in recent experiments investigating cage properties near the colloidal glass transition [17].

To be more specific, let us denote the orientation and local field correlation functions as

$$c_{m,n} = \langle \sigma_m \sigma_n \rangle, \qquad C_{m,n} = \langle h_m h_n \rangle. \tag{4.14}$$

Equation (4.6) implies

$$C_{m,n} = \sum_{k=1}^{m-1} \sum_{\ell=1}^{n-1} c_{k,\ell}, \qquad c_{m,n} = C_{m+1,n+1} - C_{m+1,n} - C_{m,n+1} + C_{m,n}, \tag{4.15}$$

and especially $c_{n,n} = C_{n+1,n+1} - 2C_{n,n+1} + C_{n,n} = 1$, so that $C_{n,n} - C_{n,n\pm1} \approx 1/2$, and more generally

$$C_{n,n} - C_{n,n+k} \approx |k|/2 \qquad (|k| \ll n). \tag{4.16}$$

The power law (4.7) and the behaviour (4.16) can be combined into the scaling Ansatz

$$C_{m,n} \approx W_m W_n \, \mathcal{F}\Big(\frac{n-m}{W_m W_n}\Big), \tag{4.17}$$

where $\mathcal{F}$ is a positive, even function, with a cusp at the origin of the form

$$\mathcal{F}(x) = 1 - |x|/2 + \cdots \qquad (|x| \ll 1). \tag{4.18}$$

As a consequence of (4.15), the orientation correlations obey a similar scaling law:

$$c_{m,n} \approx \delta_{m,n} - \frac{1}{W_m W_n} \, F\Big(\frac{n-m}{W_m W_n}\Big), \tag{4.19}$$

where $F(x) = \mathrm{d}^2\mathcal{F}/\mathrm{d}x^2$ is another positive, even function such that

$$\int_{-\infty}^{+\infty} F(x)\,\mathrm{d}x = \int_0^{+\infty} x\,F(x)\,\mathrm{d}x = 1. \tag{4.20}$$

The first of these sum rules confirms that spin fluctuations are asymptotically *totally screened*: $\sum_{m\neq n} c_{n,n} \approx -c_{n,n} = -1$. The scaling laws (4.17) and (4.19) are accurately confirmed by numerical data for $C_{m,n}$ and $c_{m,n}$, whose scaling plots are respectively shown in Figures 7 and 8.

A final consequence concerns the mixed correlation

$$\langle \sigma_n h_n \rangle = \sum_{m=1}^{n-1} c_{m,n}, \tag{4.21}$$

for which the scaling results (4.17), (4.19) yield $\langle \sigma_n h_n \rangle \approx 1/2$. Scaling then implies that the order parameter defined in (4.11) falls off as $Q_n \sim 1/W_n$, hence the estimate

$$Q_n \approx a\, n^{-1/3}. \tag{4.22}$$

This power-law decay is well confirmed by numerical data, shown in Figure 9, which yield $a \approx 0.44$.

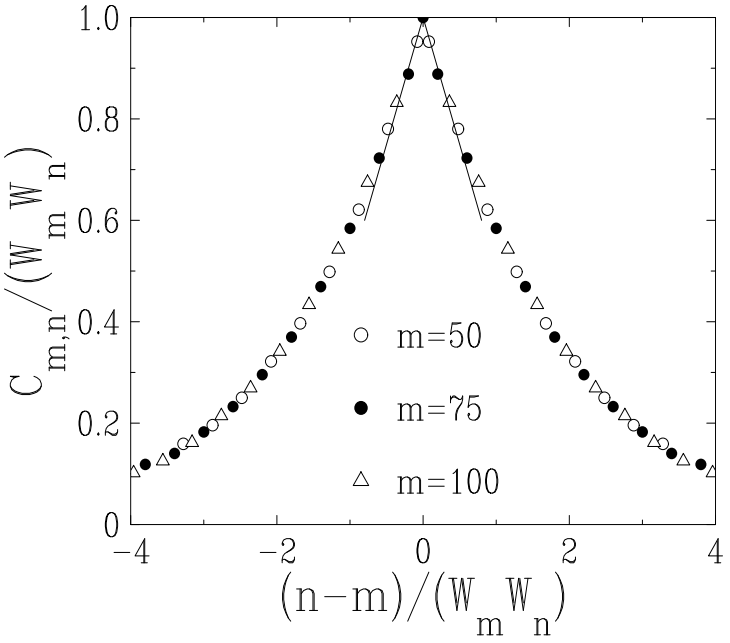


Figure 7: Scaling plot of the correlation function $C_{m,n}$ of the local fields in the zero-temperature steady state with $\varepsilon = 1$, demonstrating the validity of (4.17), and showing a plot of the scaling function $\mathcal{F}$. The full lines show the cusp behaviour (4.18).

All of the above adds up, for the case of regularly shaped grains, to a picture of grain orientations which are anticorrelated within a *dynamical cluster* [10] whose size scales as $n^{2/3}$; grains *outside* such a cluster, are orientationally screened from each other, i.e., the screening length also goes as $n^{2/3}$. (Correspondingly, from a kinetic viewpoint [16], these results may be interpreted in terms of the time $n^{2/3}$ spent by a walker bouncing back and forth between the walls of a cage, where his steps are consequently anticorrelated one with the other.) Consistently, the order parameter Q_n, proportional to the ratio of the screening length to the total length, goes as $n^{2/3}/n \sim n^{-1/3}$. By contrast, when ε is irrational, earlier orientations influence *all* successive ones, as the orientation correlations c_{mn} do not decay to zero. The order parameter is $Q_n = 1$ identically while, loosely speaking, the screening length scales as n.

Entropy

We now turn to the entropy of the steady state, defined by the usual Boltzmann formula

$$S = -\sum_{\mathcal{C}} p(\mathcal{C}) \ln p(\mathcal{C}), \tag{4.23}$$

where $p(\mathcal{C})$ is the probability that the system is in the orientation configuration $\mathcal{C}$ in the steady state, and the sum runs over all the 2^n configurations $\mathcal{C} = \{\sigma_m\}$ $(m = 1, \ldots, n)$ of a system of n grains.

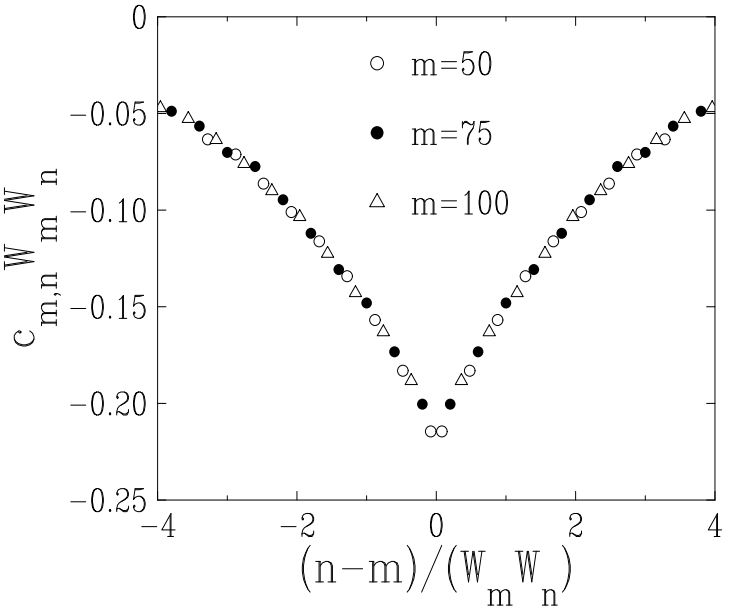


Figure 8: Scaling plot of the orientation correlation function $c_{m,n}$ for $n \neq m$ in the zero-temperature steady state with $\varepsilon = 1$, demonstrating the validity of (4.19), and showing a plot of (minus) the scaling function F (after [7]).

On the theoretical side, the entropy S can be estimated as follows, using the main feature of the zero-temperature steady state, i.e., the roughening law (4.7). Think of the depth n as a fictitious discrete time, and of the local field h_n as the position of a random walker at time n. For a free lattice random walk of n steps, one has $\langle h_n^2 \rangle = n$, and the entropy reads $S_{\text{flat}} = n \ln 2$, as all configurations are equally probable. Because $\langle h_n^2 \rangle = W_n^2 \ll n$, the entropy S of our random walk is reduced with respect to S_{flat}. Let

$$\Delta S = S_{\text{flat}} - S = n \ln 2 - S \tag{4.24}$$

be the entropy reduction [18]. Consider first a strict constraint $|h_n| < L$. The probability that a random walk of n steps obeys this constraint is known to fall off exponentially, as $\mathcal{P}_n \approx \exp(-\pi^2 n/(2L^2))$. For a slowly time-dependent constraint $|h_n| < L_n$, this estimate generalises to

$$\mathcal{P}_n \approx \exp\left(-\frac{\pi^2}{2} \sum_{m=1}^{n} \frac{1}{L_m^2}\right). \tag{4.25}$$

With the assumption that the strict constraint $|h_n| < W_n$ and the weak constraint $\langle h_n^2 \rangle = W_n$ generate similar entropy reductions for similar constraint profiles, we obtain the estimate

$$\Delta S = -\ln \mathcal{P}_n \sim \sum_{m=1}^{n} \frac{1}{W_m^2} \sim n^{1/3}. \tag{4.26}$$

We have evaluated the steady-state entropy S in a numerical simulation, using its definition (4.23), by measuring the probabilities $p(\mathcal{C})$ of all the configurations. As there

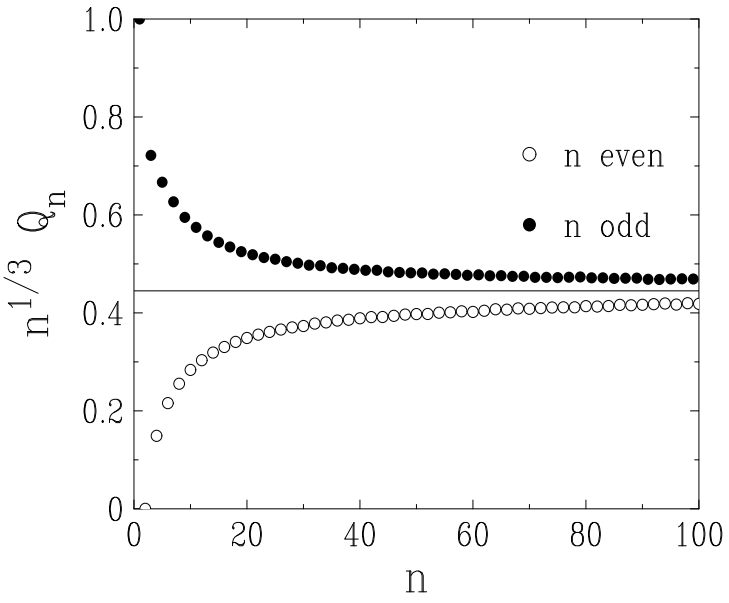


Figure 9: Plot of $n^{1/3}$ times the order parameter Q_n against n, for the zero-temperature steady state with $\varepsilon = 1$, Symbols: numerical data. Full line: common limit value, yielding $a \approx 0.44$ in (4.22).

are 2^n configurations for a system of n grains, the a priori statistical error only decays as $(2^n/t)^{1/2}$. Reliable data are obtained in this way for $t \sim 10^9$ and $n \approx 20$. Figure 10 shows a plot of the entropy reduction ΔS against n. The data show that ΔS is small, at least for system sizes reachable by numerical simulations. For $n = 12$ (data of Figure 11) we have $\Delta S \approx 0.479$. A reasonable semi-quantitative agreement with the estimate (4.26) is found: the fit shown in the plot suggests that (4.26) is affected by a logarithmic correction (which cannot be explained by the simple argument given above), with a small amplitude around 0.06.

Figure 11 shows the normalised probabilities $2^{12}\, p(\mathcal{C})$, plotted against the $2^{12} = 4096$ configurations $\mathcal{C}$ of a column of 12 grains, sorted according to lexicographical order (read down the column). This plot exhibits a startlingly rugged structure on this microscopic scale: some configurations are clearly visited far more often than others. It turns out that the most visited configurations are the $2^6 = 64$ ground states of the system (empty circles). We suggest that this behaviour is generic: i.e., *the dynamics of compaction in the jammed state leads to a microscopic sampling of configuration space which is highly non-uniform, and reflects the structure of the ground states.* In spite of this fine structure, the entropy reduction $\Delta S \sim n^{1/3}$ is subextensive, and therefore negligible with respect to the free entropy $S_{\text{flat}} = n \ln 2$, in qualitative agreement with Edwards' flatness hypothesis [1, 19]. Our model thus provides a natural reconciliation between the intuitive perception that not all configurations can be equally visited in the jammed state where compaction is favoured, and the flatness hypothesis of Edwards, which is eminently sensible for macroscopically large systems.

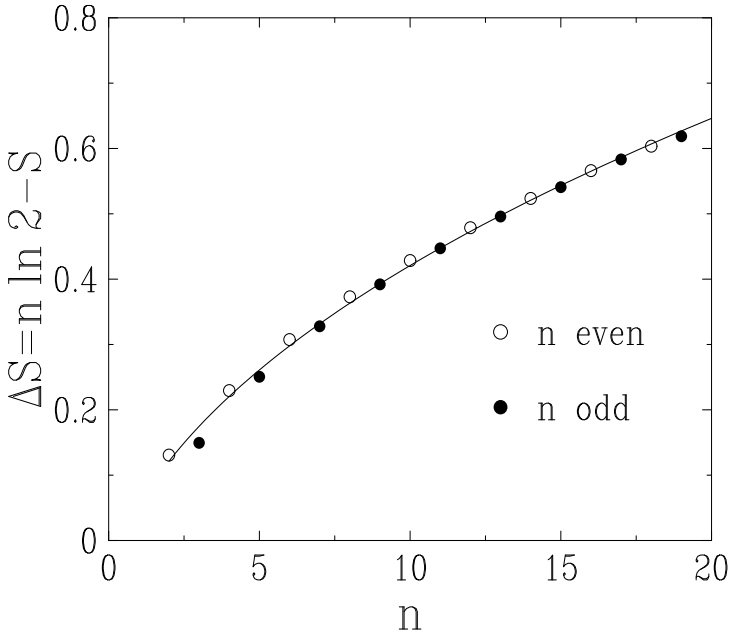


Figure 10: Plot of the measured entropy reduction ΔS in the zero-temperature steady state with $\varepsilon = 1$, defined in (4.24), against $n \leq 19$. Symbols: numerical data. Full line: fit $\Delta S = (62 \ln n + 53) 10^{-3}\, n^{1/3}$.

4.4 Rational ε, finite $\xi_{\rm dyn}$: crossover to Brownian roughening

In the case where $\xi_{\rm dyn}$ is finite, the system still relaxes to a non-trivial steady state, which is qualitatively similar to that obtained for $\xi_{\rm dyn} = \infty$, investigated above.

At the quantitative level, the main effect of the finiteness of $\xi_{\rm dyn}$ is to induce a nontrivial profile of W_n^2. In the regime where both n and $\xi_{\rm dyn}$ are large, the following scaling law is observed

$$W_n^2 \approx (W_n^2)_\infty \, f(n/\xi_{\rm dyn}), \tag{4.27}$$

where $(W_n^2)_\infty$ is given by the anomalous roughening law (4.7) of the $\xi_{\rm dyn} = \infty$ steady state, which holds more generally for $n \ll \xi_{\rm dyn}$, so that $f(0) = 1$.

A qualitative understanding of the scaling function f can be obtained by generalising the above Markovian approximation. The expression (4.12) for the strength of the noise is readily replaced by

$$D_n \approx \frac{b}{\sqrt{2\pi}} \sum_{m=1}^{n-1} \frac{\mathrm{e}^{-m/\xi_{\rm dyn}}}{W_m}. \tag{4.28}$$

For the deterministic part, (4.5) implies

$$\mathrm{d}\langle h_n \rangle / \mathrm{d}t = \sum_{m=1}^{n-1} \langle \sigma_m - \mathrm{sign}\, h_m \rangle \, \mathrm{e}^{-m/\xi_{\rm dyn}}. \tag{4.29}$$

The right-hand side is not simply related to h_n any more, so that a further level of

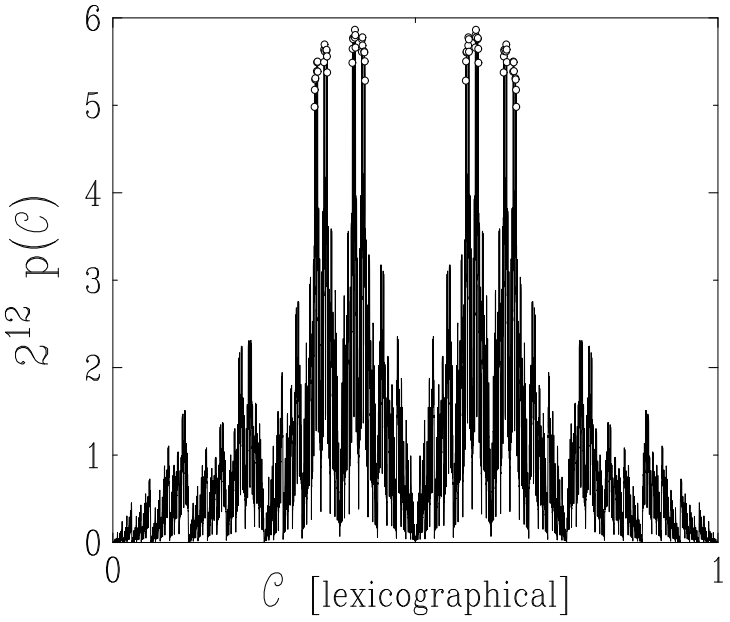


Figure 11: Plot of the normalised probabilities $2^{12}\,p(\mathcal{C})$ of the configurations of a column of 12 grains in the zero-temperature steady state with $\varepsilon = 1$, against the configurations $\mathcal{C}$ in lexicographical order. The open circles mark the $2^6 = 64$ ground-state configurations, which turn out to be the most probable (after [7]).

approximation is needed. The most straightforward choice reads

$$a_n \approx \frac{1}{n}\sum_{m=1}^{n-1} \mathrm{e}^{-m/\xi_{\mathrm{dyn}}} \approx \frac{\xi_{\mathrm{dyn}}}{n}(1-\mathrm{e}^{-n/\xi_{\mathrm{dyn}}}). \tag{4.30}$$

Skipping the derivation, we mention that (4.28), (4.30) imply (4.27), with

$$f(x) = \frac{x^{1/3}}{1-\mathrm{e}^{-x}}\left(\int_0^x (1-\mathrm{e}^{-y})^{1/2}\, y^{-1/2}\, \mathrm{e}^{-y}\,\mathrm{d}y\right)^{2/3} \approx \begin{cases} 1+x/12 & (x \ll 1), \\ K\,x^{1/3} & (x \gg 1), \end{cases} \tag{4.31}$$

and $K = 0.87732$. In view of the crudeness of the above assumptions, (4.31) is only meant to provide a qualitative description of the scaling function f. Its asymptotic behaviour for $x \gg 1$ is, however, expected to yield the correct dependence

$$W_n^2 \approx AK\xi_{\mathrm{dyn}}^{-1/3} n \tag{4.32}$$

of the width W_n on n and ξ_{dyn}. The profile of local fields is thus predicted to be Brownian for $n \gg \xi_{\mathrm{dyn}}$. Figure 12 shows a scaling plot of numerical data for the ratio $W_n^2/(W_n^2)_\infty$, against $x = n/\xi_{\mathrm{dyn}}$. A scaling law of the form (4.27) is clearly observed. The fitted curve is compatible with (4.32), with $K \approx 2.66$.

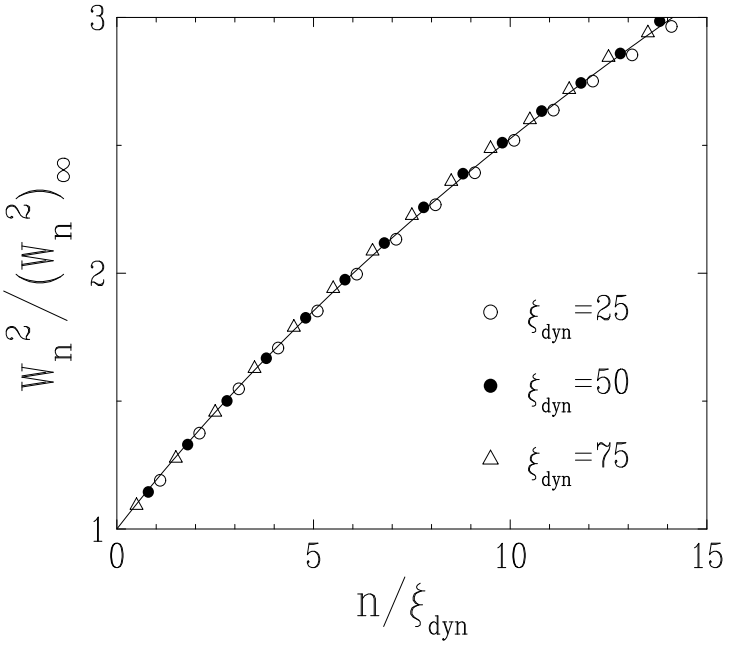


Figure 12: Scaling plot of the ratio $W_n^2/(W_n^2)_\infty$ against $x = n/\xi_{\rm dyn}$ in the zero-temperature steady state with $\varepsilon = 1$, illustrating the scaling law (4.27), and showing a plot of the scaling function f. Symbols: numerical data. Curve: fit $f = 1 + a((1 + bx)^{1/3} - 1)$, with $a = 5.63$, $b = 0.105$, so that $K = a\, b^{1/3} = 2.66$.

5 Low-temperature dynamics

We now turn to the investigation of the low-temperature dynamics of the model. Our main findings are the observation of *intermittency* in the position of the boundary layer; this has recently been observed in experiments of vibrated granular beds [20].

We consider for simplicity the case of an infinite $\xi_{\rm dyn}$. If the slope ε is irrational, the dynamical rule (4.1) is fully deterministic at zero temperature, so that a small non-zero temperature is expected to have drastic effects. To the contrary, for a rational slope ε, the rule (4.5) is already stochastic at zero temperature, and indeed no interesting effect appears at a small non-zero temperature.

We therefore focus our attention onto the case of an irrational slope ε. We recall that the zero-temperature dynamics drives the system to its unique quasiperiodic ground state, where each orientation is aligned with its local field, according to (3.2). For a low but non-zero temperature Γ, there will be *mistakes*, i.e., orientations $\sigma_n = -\operatorname{sign} h_n$ not aligned with their local field. Equation (3.1) suggests that the a priori probability of observing a mistake at site n scales as

$$\Pi(n) \approx \exp(-2|h_n|/\Gamma). \tag{5.1}$$

Hence the sites n such that the local field h_n is relatively small in the ground state ($|h_n| \sim \Gamma \ll 1$) will be nucleation sites for mistakes, and thus govern the low-temperature dynamics, in a sense that will become more precise.

The leading nucleation sites can be located as follows. Equation (3.6) shows that the local field h_n is small when $n\Omega$ is close to an integer m. The latter turns out to be $m = m_n^+$. Indeed

$$n\Omega = m + \delta \Longrightarrow h_n = \delta/(1-\Omega) \tag{5.2}$$

for δ small enough ($\Omega - 1 < \delta < \Omega$). The leading nucleation sites therefore correspond to the rational numbers m/n which are the closest to the irrational rotation number Ω. This is a well-defined problem of Number Theory, referred to as the Diophantine approximation [13].

5.1 The golden-mean slope

Before we tackle the problem in general, we consider again for definiteness the golden-mean slope (3.9). In this case, we are led to introduce the Fibonacci numbers F_k [12, 13], defined by the recursion formula

$$F_k = F_{k-1} + F_{k-2} \qquad (F_0 = 0, \quad F_1 = 1). \tag{5.3}$$

We have alternatively

$$F_k = \frac{\Phi^k - (-\Phi)^{-k}}{\sqrt{5}}. \tag{5.4}$$

The leading nucleation sites are the Fibonacci sites $n = F_k$. We have $m = m_n^+ = F_{k-2}$, $m_n^- = F_{k-1}$, and

$$h_n = (-)^k \, \Phi^{-(k-1)}, \tag{5.5}$$

so that

$$\Pi_k = \Pi(F_k) \sim \exp\left(-\frac{2\Phi}{\sqrt{5}\,\Gamma F_k}\right). \tag{5.6}$$

We can therefore draw the following picture of low-temperature dynamics. Mistakes are nucleated at Fibonacci sites, according to a Poisson process. They are then advected with constant velocity $V \approx 2.58$, just as in the zero-temperature case. The system is ordered according to its quasiperiodic ground state in an upper layer ($n < \mathcal{N}(t)$), while the rest is disordered, somehow like the zero-temperature steady state for a rational slope. The depth $\mathcal{N}(t)$ of the ordered layer, given by the position of the *uppermost* mistake, is a collective co-ordinate describing low-temperature dynamics. It evolves according to ballistic advection, i.e., $\mathcal{N}(t_1) = \mathcal{N}(t_0) + V(t_1 - t_0)$, until it jumps backward to a smaller depth $\mathcal{N}(t_1) = F_k$, if another mistake is nucleated there. Figure 13 shows a typical sawtooth plot of the instantaneous depth $\mathcal{N}(t)$, for a temperature $\Gamma = 0.003$. The leading nucleation sites are observed to be given by Fibonacci numbers.

The system thus reaches a steady state, characterised by a finite ordering length $\langle \mathcal{N} \rangle$, which diverges at low temperature, as mistakes become more and more rare. The law of this divergence can be predicted by the following argument. The most active nucleation

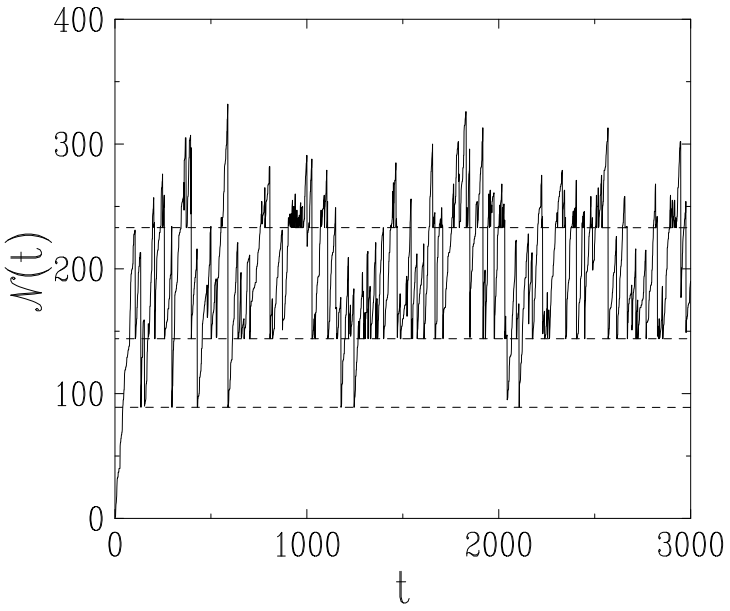


Figure 13: Plot of the instantaneous depth $\mathcal{N}(t)$ of the ordered layer, for the golden-mean slope at $\Gamma = 0.003$. Dashed lines: leading nucleation sites given by consecutive Fibonacci numbers (bottom to top: $F_{11} = 89$, $F_{12} = 144$, $F_{13} = 233$) (after [7]).

Fibonacci site is such that the nucleation time $1/\Pi_k$ is comparable to the advection time to the next nucleation site F_{k+1}, i.e., $(F_{k+1} - F_k)/V \approx F_k/(\Phi V)$, hence the estimate

$$\frac{\Pi_k F_k}{\Phi V} \sim 1. \tag{5.7}$$

Indeed, less deep sites have too small nucleation rates, while the mistakes nucleated at deeper sites have little chance to be the uppermost ones. Equations (5.6) and (5.7) yield

$$\frac{\sqrt{5}}{2\Phi}\,\Gamma F_k \ln \frac{F_k}{\Phi V} \sim 1. \tag{5.8}$$

For $\Gamma = 0.003$, and for the Fibonacci sites shown in Figure 13, the left-hand side of (5.8) respectively reads 0.56 for $F_{11} = 89$, 1.06 for $F_{12} = 144$, and 1.94 for $F_{13} = 233$. The estimate (5.8) therefore correctly predicts the observed fact that $F_{12} = 144$ is the most active nucleation site at that temperature.

The heuristic argument leading to (5.8) can be justified and made more precise by means of the results of Appendix A. The continuum approach used there is justified because the Fibonacci sites are more and more sparse. In the case of present interest, keeping only the Fibonacci sequence of leading nucleation sites, we obtain the prediction (A.6) for the ordering length, to be shown in Figure 14.

For a low enough temperature Γ, the sum entering the right-hand side of (A.6) is sharply cutoff. It can indeed be argued that the term of order k in that sum is essentially F_{k-1} for $k \leq k^\star$, while it is exponentially negligible for $k \geq k^\star + 1$, where $k^\star = \mathrm{Int}(K)$,

and K is the *real* solution of (5.8), considered as a strict equality, with $F_K \approx \Phi^K/\sqrt{5}$, according to (5.4). We have therefore $\langle \mathcal{N} \rangle \approx F_{k^\star+1}$, i.e., more explicitly,

$$\langle \mathcal{N} \rangle \approx F_K \, \mathcal{A}_K. \tag{5.9}$$

The first factor of this expression,

$$F_K \approx \frac{2\Phi}{\sqrt{5}\,\Gamma|\ln\Gamma|} \left(1 - \frac{1}{|\ln\Gamma|} \, \ln \frac{2\Phi}{\sqrt{5} V |\ln\Gamma|} + \cdots \right), \tag{5.10}$$

shows that the ordering length obeys a linear divergence at low temperature, with explicit logarithmic corrections. The second factor,

$$\mathcal{A}_K = \Phi^{1-\mathrm{Frac}(K)}, \tag{5.11}$$

is a periodic function of its argument $K \approx |\ln\Gamma|/\ln\Phi$, with unit period, which oscillates between the bounds $\mathcal{A}_{\max} = \Phi$ and $\mathcal{A}_{\min} = 1$. *Oscillatory amplitudes* are commonly observed in models related to self-similar structures [21]; they originate in the discrete self-similarity of the underlying sequence. The oscillations of the asymptotic amplitude $\mathcal{A}_K$, given in (5.11), are damped, except at extremely low temperature. Figure 14 shows a plot of numerical data for the product $\Gamma\langle \mathcal{N} \rangle$, against $|\ln\Gamma|$. These data are well described by the analytical prediction (A.6), and lie within the bounds of the asymptotic estimate (5.9)–(5.11). The oscillations become visible on the analytical curve for the lower temperatures ($\Gamma < 10^{-4}$), which are not directly accessible to simulations.

5.2 Other irrational slopes

We now consider briefly the case of an arbitrary irrational slope ε. The situation is rather similar to the phenomenon of hierarchical melting, observed at low temperature in some incommensurate modulated solids [22].

The nucleation sites can be determined as follows. The irrational rotation number Ω can be written as an infinite *continued-fraction expansion* [13]:

$$\Omega = \cfrac{1}{a_1 + \cfrac{1}{a_2 + \cfrac{1}{a_3 + \cdots}}} = [a_1, a_2, a_3, \ldots]. \tag{5.12}$$

The principal approximants of Ω are the rationals

$$\Omega_k = p_k/q_k, \tag{5.13}$$

whose numerators and denominators obey the same linear recursion

$$p_k = a_k p_{k-1} + p_{k-2}, \qquad q_k = a_k q_{k-1} + q_{k-2}, \tag{5.14}$$

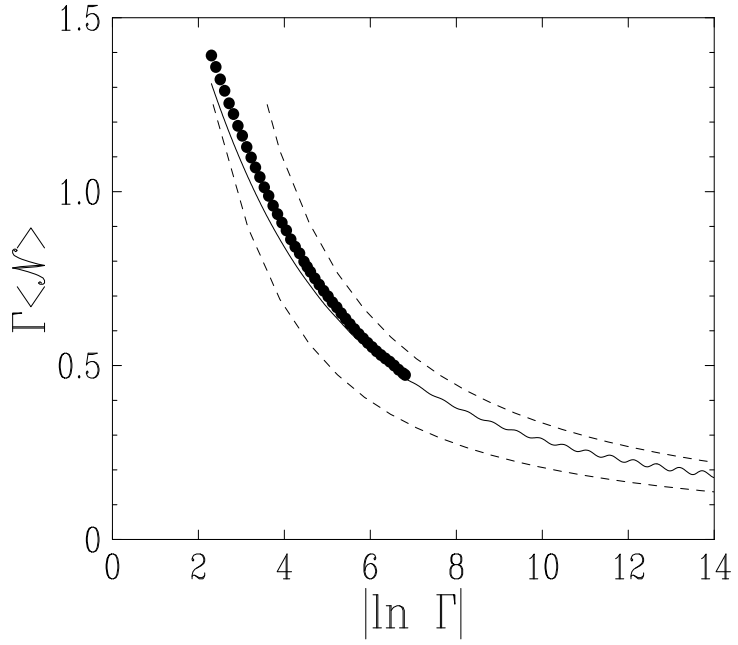


Figure 14: Plot of the product $\Gamma\langle\mathcal{N}\rangle$ against $|\ln\Gamma|$, for the golden-mean slope. Symbols: numerical data. Full line: analytical prediction (A.6). Dashed lines: Extrema of the asymptotic result (5.9), corresponding to $\mathcal{A} = \mathcal{A}_{\max}$ (upper curve) and $\mathcal{A} = \mathcal{A}_{\min}$ (lower curve).

with $p_0 = q_{-1} = 0$, $p_1 = q_0 = 1$. The denominators build the leading sequence of nucleation sites. The rotation number Ω also has secondary approximants

$$\Omega_{k,b} = (bp_{k-1} + p_{k-2})/(bq_{k-1} + q_{k-2}) \tag{5.15}$$

for $b = 1, \ldots, a_k - 1$ if $a_k > 1$. The denominators are the subleading nucleation sites.

For the golden-mean slope, we have $\Omega = 2 - \Phi = [2, 1, 1, 1, 1, \ldots]$, so that the leading Fibonacci nucleation sites of section 5.1 are recovered, whereas there are no subleading nucleation sites.

The most active nucleation site at low temperature can again be estimated by comparing the nucleation time and the advection time. The ordering length $\langle\mathcal{N}\rangle$ is thus still predicted to diverge as

$$\langle\mathcal{N}\rangle \approx \frac{\mathcal{A}(\ln\Gamma)}{\Gamma|\ln\Gamma|}, \tag{5.16}$$

at least for irrational numbers with typical Diophantine properties. Most irrational numbers are typical in this respect. The presence of secondary approximants makes however the oscillation pattern of the amplitude $\mathcal{A}(\ln\Gamma)$ more complex than a simple periodic function in general, in analogy with the low-temperature specific heat peaks induced by hierarchical melting [22].

In more physical terms, the ordering length $\langle\mathcal{N}\rangle$ defines the mean position of an *intermittent* boundary layer, separating an ordered state above it from a disordered

state below. This length is thus a kind of finite-temperature equivalent of the 'zero-temperature' length $\xi_{\rm dyn}$. Both $\langle \mathcal{N} \rangle$ and $\xi_{\rm dyn}$ retain the flavour of a boundary layer separating order from disorder. Within each of these boundary layers, the relaxation is *fast*, and based on single-particle relaxation, i.e., individual particles attaining their positions of optimal local packing [10, 23]. The *slow* dynamics of cooperative relaxation only sets in for lengths *beyond* these, when the moves by which packing needs to be optimised become non-local.

6 Discussion

The work we have presented here concerns the effect of shape on compaction properties of grains. If irrational and rational values of ε, the volume occupied by a disordered grain, are taken to correspond to irregular and regular grains, we see a distinct difference in behaviour between the two.

While the uniqueness of packing of irregular grains in their ground state vis-a-vis the degeneracy of perfectly packed ground states for regularly shaped grains is in accord with intuition, the effect of dynamics is more subtle. The fact that the perfectly packed and degenerate ground states of the regular grains are *never* retrieved by zero-temperature dynamics, leading instead to density fluctuations (that have been observed experimentally [9]) is rather subtle, as compared with the less perfect, unique and perfectly retrievable ground state for the irregular grains. Clearly, a sharp distinction between neighbouring rational and irrational values of ε only makes sense for an infinitely deep system. For a finite column made of N grains, the distinction is rounded off by finite-size effects. In particular, the characteristic features of any 'large' rational ε are no longer observed when the period $p + q$ becomes larger than N.

Zero-temperature steady-state density fluctuations for regular grains are subextensive: grain orientations are thus *fully anticorrelated*, reminiscent of dynamical heterogeneities in bridge collapse [10] in strongly compacted granular media, as well as temporal anticorrelations in cages [16, 17]. Also, while the macroscopic entropy of the steady state [18] is approximately that of a fully disordered column, consistent with Edwards' 'flatness' hypothesis [1], a microscopic examination of the configurations reveals a rugged landscape, with the most visited configurations corresponding to the ground states. As a matter of fact, the steady-state fluctuations of the local fields remain subextensive at any finite temperature. As a consequence, after a short transient regime, the steady-state proportions of ordered and disordered grains are solely determined by ε, and given by (3.8), for both rational and irrational values of ε.

Lastly, the low-temperature dynamics for irrational ε leads to an intermittency of the surface layer. We would expect that for large enough temperatures, there would be little distinction between regular and irregular grains; our model however provides an interesting prediction of boundary-layer intermittency, which should be visible at low enough temperatures for irregularly shaped objects.

Acknowledgements

AM warmly acknowledges the hospitality of the Service de Physique Théorique, Saclay, where most of this work was conceived.

A Distribution of the depth $\mathcal{N}$ of the upper layer

This Appendix is devoted to the depth $\mathcal{N}(t)$ of the ordered layer for low-temperature dynamics in the irrational case. Our main goal is to derive the stationary distribution of $\mathcal{N}$, for the effective dynamics described in section 5.1.

For convenience we use a continuous formalism, treating $\mathcal{N}$ as a real variable. Let $\pi(x)\,\mathrm{d}x$ be the given nucleation rate per unit time between x and $x+\mathrm{d}x$, and $p(x,t)\,\mathrm{d}x$ be the probability of finding the depth $\mathcal{N}$ between x and $x+\mathrm{d}x$ at time t. The unknown probability distribution function $p(x,t)$ obeys the rate equation

$$\left(\frac{\partial}{\partial t}+V\frac{\partial}{\partial x}\right)p(x,t)=\pi(x)P(x,t)-p(x,t)\Pi(x)\equiv\frac{\partial}{\partial x}\Big(\Pi(x)P(x,t)\Big), \tag{A.1}$$

with the notations

$$P(x,t)=\int_x^\infty p(y,t)\,\mathrm{d}y,\quad p(x,t)=-\frac{\partial P(x,t)}{\partial x},\quad \Pi(x)=\int_0^x \pi(y)\,\mathrm{d}y,\quad \pi(x)=\frac{\mathrm{d}\Pi(x)}{\mathrm{d}x}. \tag{A.2}$$

Indeed, the left-hand side of (A.1) is the usual covariant derivative, whose convective term involves the drift velocity V. The middle side represents the evolution due to nucleation events, with the first (gain) term originating in nucleation at depth x, and the second (loss) term originating in nucleation at depth $y<x$.

The stationary (time-independent) solution $p_{\mathrm{stat}}(x)$ of (A.1) is such that

$$V\,p_{\mathrm{stat}}(x)\equiv -V\,\frac{\mathrm{d}P_{\mathrm{stat}}(x)}{\mathrm{d}x}=\Pi(x)P_{\mathrm{stat}}(x). \tag{A.3}$$

This separable differential equation easily yields the results

$$P_{\mathrm{stat}}(x)=\exp\left(-\frac{1}{V}\int_0^x\Pi(y)\,\mathrm{d}y\right),\quad p_{\mathrm{stat}}(x)=\frac{\Pi(x)}{V}\exp\left(-\frac{1}{V}\int_0^x\Pi(y)\,\mathrm{d}y\right), \tag{A.4}$$

and especially

$$\langle\mathcal{N}\rangle=\int_0^\infty\exp\left(-\frac{1}{V}\int_0^x\Pi(y)\,\mathrm{d}y\right)\mathrm{d}x=\int_0^\infty\exp\left(-\frac{1}{V}\int_0^x(x-y)\pi(y)\,\mathrm{d}y\right)\mathrm{d}x. \tag{A.5}$$

These expressions hold for an arbitrary distribution of nucleation rates.

In the case of interest in section 5.1, taking into account the leading sequence of Fibonacci sites F_k, with nucleation rates Π_k, we obtain

$$\langle\mathcal{N}\rangle=\sum_{k=0}^\infty\frac{V}{A_k}\,\left(\mathrm{e}^{-B_k/V}-\mathrm{e}^{-B_{k+1}/V}\right), \tag{A.6}$$

with

$$A_k=\sum_{\ell=0}^{k}\Pi_\ell,\quad B_k=\sum_{\ell=0}^{k-1}(F_k-F_\ell)\Pi_\ell. \tag{A.7}$$

References

[1] S.F. Edwards, in *Granular Matter: An Interdisciplinary Approach*, ed. A. Mehta (Springer, New York, 1994).

[2] P.G. de Gennes, Rev. Mod. Phys. **71**, S374 (1999).

[3] M.F. Shlesinger and J.T. Bendler, in *Phase Transitions in Soft Condensed Matter*, T. Riste and D. Sherrington, eds. (Plenum, 1989); R. Monasson, Phys. Rev. Lett. **75**, 2847 (1995); E. Marinari, G. Parisi, F. Ricci-Tersenghi, and F. Zuliani, J. Phys. A **34**, 383 (2001); L. Berthier, L.F. Cugliandolo, and J.L. Iguain, Phys. Rev. E **63**, 051302 (2001); M. Mézard, Physica A **306**, 25 (2002); G. Biroli and M. Mézard, Phys. Rev. Lett. **88**, 025501 (2002); A. Lawlor, D. Reagan, G.D. McCullagh, P. De Gregorio, P. Tartaglia, and K.A. Dawson, Phys. Rev. Lett. **89**, 245503 (2002).

[4] M. Mézard, G. Parisi, and M.A. Virasoro, *Spin Glass Theory and Beyond* (World Scientific, Singapore, 1987).

[5] P.F. Stadler, J.M. Luck, and A. Mehta, Europhys. Lett. **57**, 46 (2002).

[6] P.F. Stadler, A. Mehta, and J.M. Luck, Adv. Complex Systems **4**, 429 (2001).

[7] A. Mehta and J.M. Luck, J. Phys. A **36**, L365 (2003).

[8] J.D. Bernal, Proc. R. Soc. London A **280**, 299 (1964).

[9] E.R. Nowak, J.B. Knight, M. Povinelli, H.M. Jaeger, and S.R. Nagel, Powder Technology **94**, 79 (1997); E.R. Nowak, J.B. Knight, E. Ben-Naim, H.M. Jaeger, and S.R. Nagel, Phys. Rev. E **57**, 1971 (1998); E.R. Nowak, A. Grushin, A.C.B. Barnum, and M.B. Weissman, Phys. Rev. E **63**, 020301 (2001).

[10] A. Mehta and G.C. Barker, Phys. Rev. Lett. **67**, 394 (1991); G.C. Barker and A. Mehta, Phys. Rev. A **45**, 3435 (1992); Phys. Rev. E **47**, 184 (1993); A. Mehta and G.C. Barker, Europhys. Lett. **27**, 501 (1994); J. Phys. Cond. Matt. **12**, 6619 (2000).

[11] R.L. Brown and J.C. Richards, *Principles of Powder Mechanics* (Pergamon, Oxford, 1970).

[12] N.G. de Bruijn, Nederl. Akad. Wetens. Proc. A **84**, 27 (1981); M. Duneau and A. Katz, Phys. Rev. Lett. **54**, 2688 (1985); J. Phys. (France) **47**, 181 (1986); V. Elser, Phys. Rev. B **32**, 4892 (1985); P.A. Kalugin, A.Yu. Kitayev, and L.S. Levitov, JETP Lett. **41**, 145 (1985); J. Phys. (France) Lett. **46**, L601 (1985).

[13] G.H. Hardy and E.M. Wright, *An Introduction to the Theory of Numbers* (Clarendon, Oxford, 1990).

[14] A.J. Bray, Adv. Phys. **43**, 357 (1994).

[15] R. Cordery, S. Sarker, and J. Tobochnik, Phys. Rev. B **24**, 5402 (1981); S.J. Cornell, K. Kaski, and R.B. Stinchcombe, Phys. Rev. B **44**, 12263 (1991); S.J. Cornell and A.J. Bray, Phys. Rev. E **54**, 1153 (1996); V. Spirin, P.L. Krapivsky, and S. Redner, Phys. Rev. E **60**, 2670 (1999).

[16] A.J. Moreno and W. Kob, preprint cond-mat/0303510; W. Kob, talk at *Unifying concepts in granular media and glasses* (Anacapri, Capri, Italy, June 25–28, 2003), and private communication.

[17] E.R. Weeks and D.A. Weitz, Chem. Phys. **284**, 361 (2002).

[18] R. Monasson and O. Pouliquen, Physica A **236**, 395 (1997).

[19] S.F. Edwards and D.V. Grinev, Phys. Rev. E **58**, 4758 (1999).

[20] E. Clément and A. Lindner, private communication.

[21] J.M. Luck, C. Godrèche, A. Janner, and T. Janssen, J. Phys. A **26**, 1951 (1993); J.M. Luck, in *Fundamental Problems in Statistical Mechanics VIII*, eds. H. van Beijeren and M.H. Ernst (Elsevier, Amsterdam, 1994).

[22] F. Vallet, R. Schilling, and S. Aubry, Europhys. Lett. **2**, 815 (1986); R. Schilling and S. Aubry, J. Phys. C **20**, 4881 (1987); F. Vallet, R. Schilling, and S. Aubry, J. Phys. C **21**, 67 (1988).

[23] J. Berg and A. Mehta, Europhys. Lett. **56**, 784 (2001); Phys. Rev. E **65**, 031305 (2002).